Improved Detection Using Negative Elevation Angles for Mountaintop WSR-88Ds: Simulation of KMSX near Missoula, Montana

RODGER A. BROWN AND VINCENT T. WOOD

National Severe Storms Laboratory, Norman, Oklahoma

TIMOTHY W. BARKER*

National Weather Service Forecast Office, Missoula, Montana

(Manuscript received 21 May 2001, in final form 12 October 2001)

ABSTRACT

KMSX, near Missoula, Montana, is one of the Weather Surveillance Radars-1988 Doppler (WSR-88Ds) that are located on the top of a mountain. Because all WSR-88Ds employ scanning strategies that were developed for flatland radars, mountaintop radars send signals well above the populated valleys and terrain surrounding the radars. Forecasters who use mountaintop WSR-88Ds are at a distinct disadvantage in not being able to detect crucial weather phenomena near the earth's surface. The use of negative elevation angles has been proposed as a solution to this problem. This type of radar operation poses no public radiation hazard, because the microwave radiation exposure level is about two orders of magnitude below the acceptable guideline near the radar and rapidly decreases with increasing distance. The feasibility of KMSX using negative elevation angles is simulated using several different weather situations. The simulations show the potential for improved detections of low-altitude weather conditions in the surrounding valleys and improved estimates of precipitation amounts throughout the coverage area. For example, using the lowest elevation angle (+0.5°) of the current WSR-88D scanning strategies, simulated rainfall rates detected in the valleys progressively decrease from about 80% of the surface value near the radar to only 1% of the surface value at 220 km. However, using an elevation angle of −0.8°, simulated rainfall rates detected at *all* ranges out to 220 km are about 80%–95% of the surface values.

1. Introduction

During the early and mid-1990s, Weather Surveillance Radar-1988 Doppler (WSR-88D) systems were installed in the United States and at selected overseas sites. Most of the radars are located on relatively flat terrain. Of those located in the more mountainous regions, many are located on the tops of hills or mountains. There are about 20 WSR-88Ds in the western states, northeastern states, Alaska, and Hawaii that would qualify as mountaintop radars. As the initial—and current—configuration, all of the WSR-88Ds have the same set of scanning strategies with +0.5° being the lowest elevation angle (e.g., Crum et al. 1993). As a consequence, mountaintop radars point well above the local population centers and do a very poor job of detecting damaging wind and precipitation events near the earth's surface.

Forecasters who use mountaintop radars express frustration in not being able to collect data closer to the ground. Acknowledging that the solution is to use negative elevation angles, the National Severe Storms Laboratory has begun a study of the potential benefits using simulated WSR-88D scanning strategies that are tailored to individual radar sites. Each mountaintop radar, then, would have its own unique set of elevation angles.

In this paper, simulated data are used to explore whether negative elevation angles might improve the detection of hazardous weather conditions and improve the estimation of precipitation using the mountaintop WSR-88D near Missoula, Montana (KMSX). In section 2, a sample mountaintop scanning strategy or ''volume coverage pattern'' (VCP) for KMSX is presented. The fact that scanning WSR-88Ds pose no microwave radiation hazard to the public is discussed in section 3. Radar-related forecasting challenges experienced by the Missoula forecast office are discussed in section 4. The results of applying the mountaintop VCP to some simulated weather situations are shown in section 5. The potential advantage of negative elevation angles for computing precipitation rates over complex terrain is

*Current affiliation: National Weather Service Forecast Office, Boise, Idaho.

Corresponding author address: Dr. Rodger A. Brown, National Severe Storms Laboratory, 1313 Halley Circle, Norman, OK 73069. E-mail: Rodger.Brown@noaa.gov

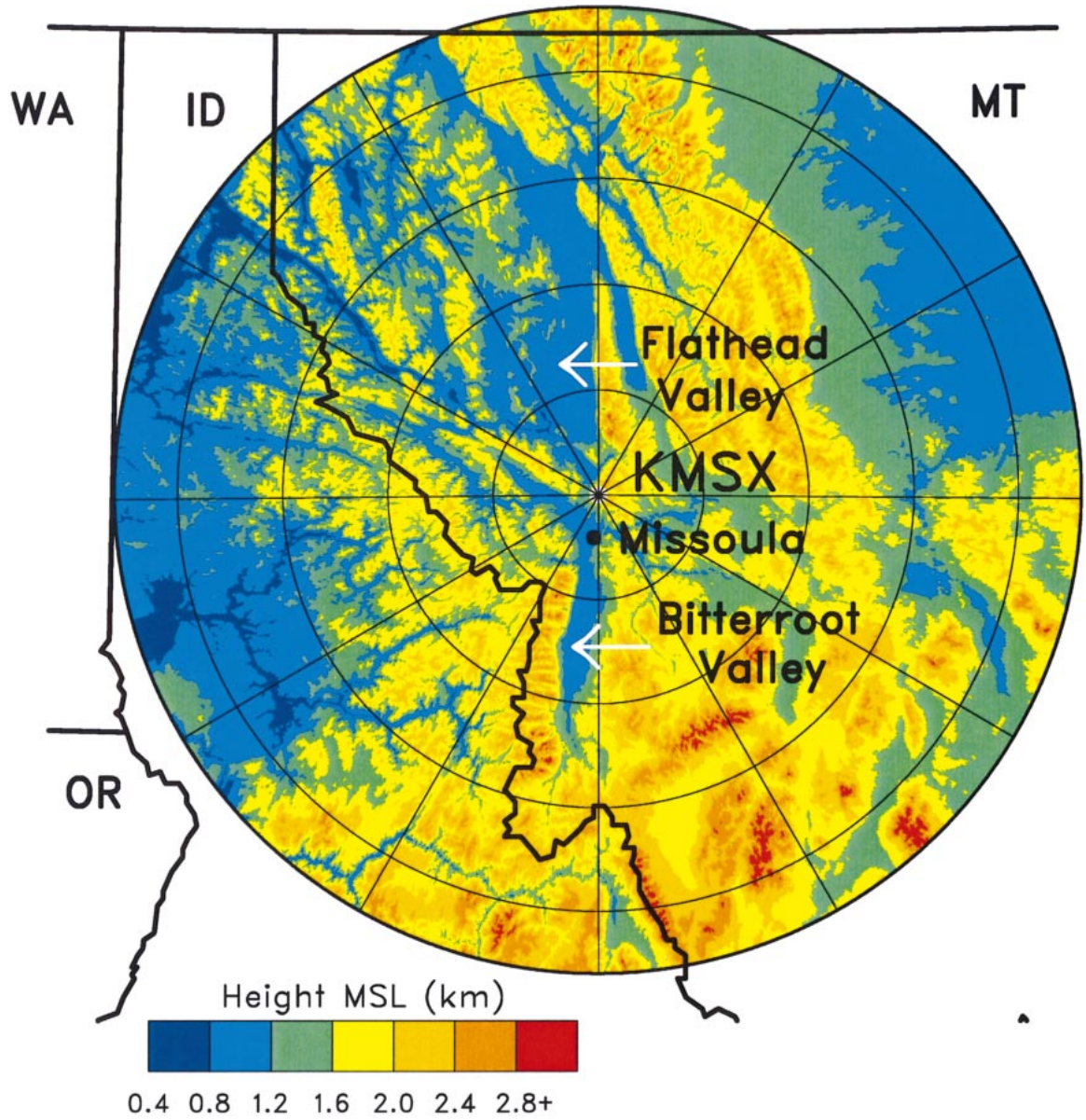

FIG. 1. Terrain within 230 km of KMSX. Range circles are at 50-km intervals. Polar coordinate terrain data courtesy of the National Weather Service's Radar Operations Center.

discussed in section 6. A concluding discussion is found in section 7.

2. Sample volume coverage pattern for KMSX

The KMSX radar is located 2.4 km above mean sea level atop Point Six Mountain about 20 km north of Missoula. Figure 1 shows the topography within 230 km of the radar. The radar was judiciously located so that it would have unobstructed views of the primary population centers in the Flathead River valley (including the Flathead Lake recreational area) to the NNW of the radar and in the Bitterroot River valley extending from Missoula to the south. [Typical site selection criteria are discussed by Leone et al. (1989).] These population centers are located about 1.5 km below the radar, as are secondary population centers within 50 km of the radar located along Interstate 90 in the Clark Fork valley to the NW and ESE of Missoula.

The procedure for developing a sample VCP for KMSX is discussed in appendix A. The lowest elevation angle of $-0.8°$ was selected so that the center of the beam would be 0.3° above a plane 1.5 km below the radar (the lowest practical elevation angle for a WSR-88D is about $-1.0°$). Vertical cross sections of this mountaintop VCP over the Flathead and Bitterroot River

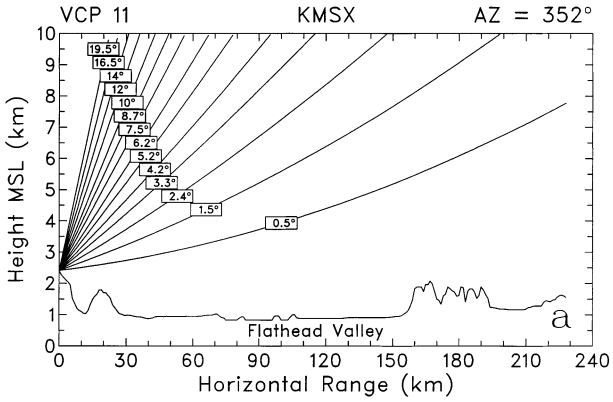

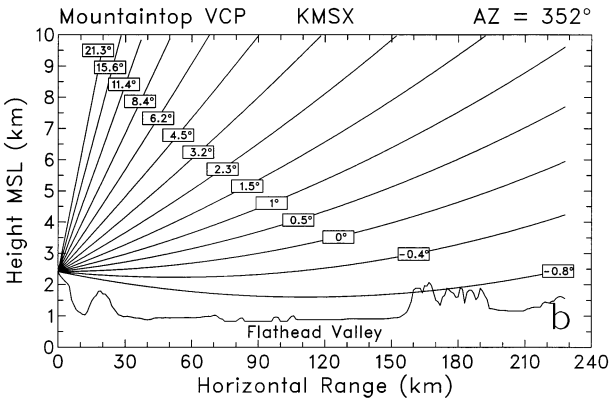

FIG. 2. Simulated vertical cross section of (a) conventional scanning strategy VCP 11 and (b) mountaintop VCP for KMSX along 352° azimuth over the Flathead River valley. Each curve indicates the center of the radar beam at the specified elevation angle. In (b), the beam at the lowest elevation angle is partially blocked by terrain with the reflectivity values being recoverable. Both VCPs complete a three-dimensional volume scan in 5 min.

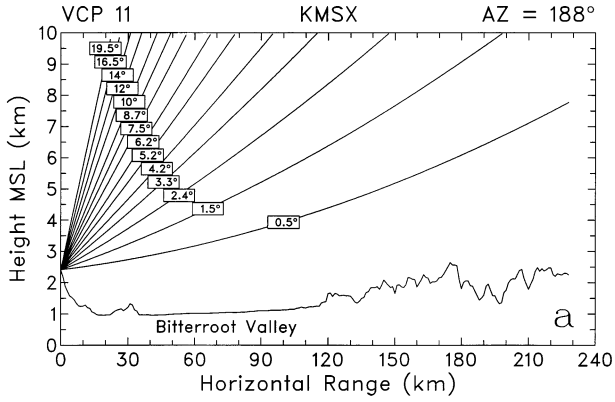

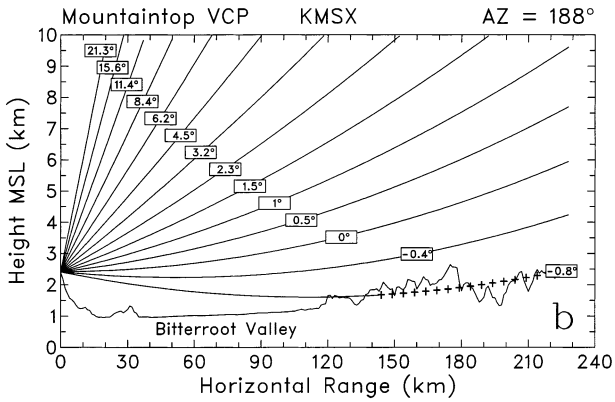

FIG. 3. Same as Fig. 2 but along azimuth 188° over the Bitterroot River valley. Plus signs indicate total beam blockage.

valleys are shown in Figs. 2b and 3b, respectively. For comparison, vertical cross sections of the current scanning strategy VCP 11 are shown in Figs. 2a and 3a. The figures indicate that negative elevation angles and the closer spacing between the lower elevation angles produce a marked potential improvement in the detection of low-altitude phenomena. For example, at ranges of 50, 100, 150, and 200 km from the radar, the mountaintop VCP would detect unobstructed features at 1.2, 2.4, 3.6, and 4.7 km lower than VCP 11 and the other current VCPs are capable of detecting.

With negative elevation angles, one would expect there to be considerable blockage by the variable terrain. For example, blockage along the 188° azimuth in the Bitterroot River valley is indicated by plus signs in Fig. 3b. The WSR-88D precipitation algorithm adjusts for partial beam blockage when converting reflectivity measurements to rainfall rates. According to Fulton et al. (1998), if 60% or less of the beam is blocked, corrections are applied to WSR-88D reflectivity measurements to approximately recover the values that would have been measured in the absence of blockage. If more than 60% of the beam is blocked, then the beam is considered to be completely blocked. The procedure for computing the percentage of beam blockage in this study is discussed in appendix B.

Figure 4 shows the lowest unblocked elevation angle for the various portions of the radar coverage area. The dark blue area indicates that the lowest elevation angle (−0.8°) covers the Flathead and Bitterroot River valleys as well as the other populated valleys within 50–100 km of the radar. With the addition of the next elevation angle (light blue area representing −0.4°), over one-half of the area within 230 km of the radar has unblocked coverage. After the 0.0° elevation angle (green) is added, the only remaining blockage is due to high peaks. With the increased amount of terrain blockage at the lower elevation angles, there may be increased challenges (over those currently encountered) concerning the suppression of radar return from the terrain.

3. Potential for microwave radiation exposure

With negative elevation angles placing the beam closer to the ground and with the beam hitting the higher nearby terrain in some locales, there is the increased potential that human beings on the ground may be exposed to microwave radiation. To safeguard the public, the Federal Communications Commission (FCC) has

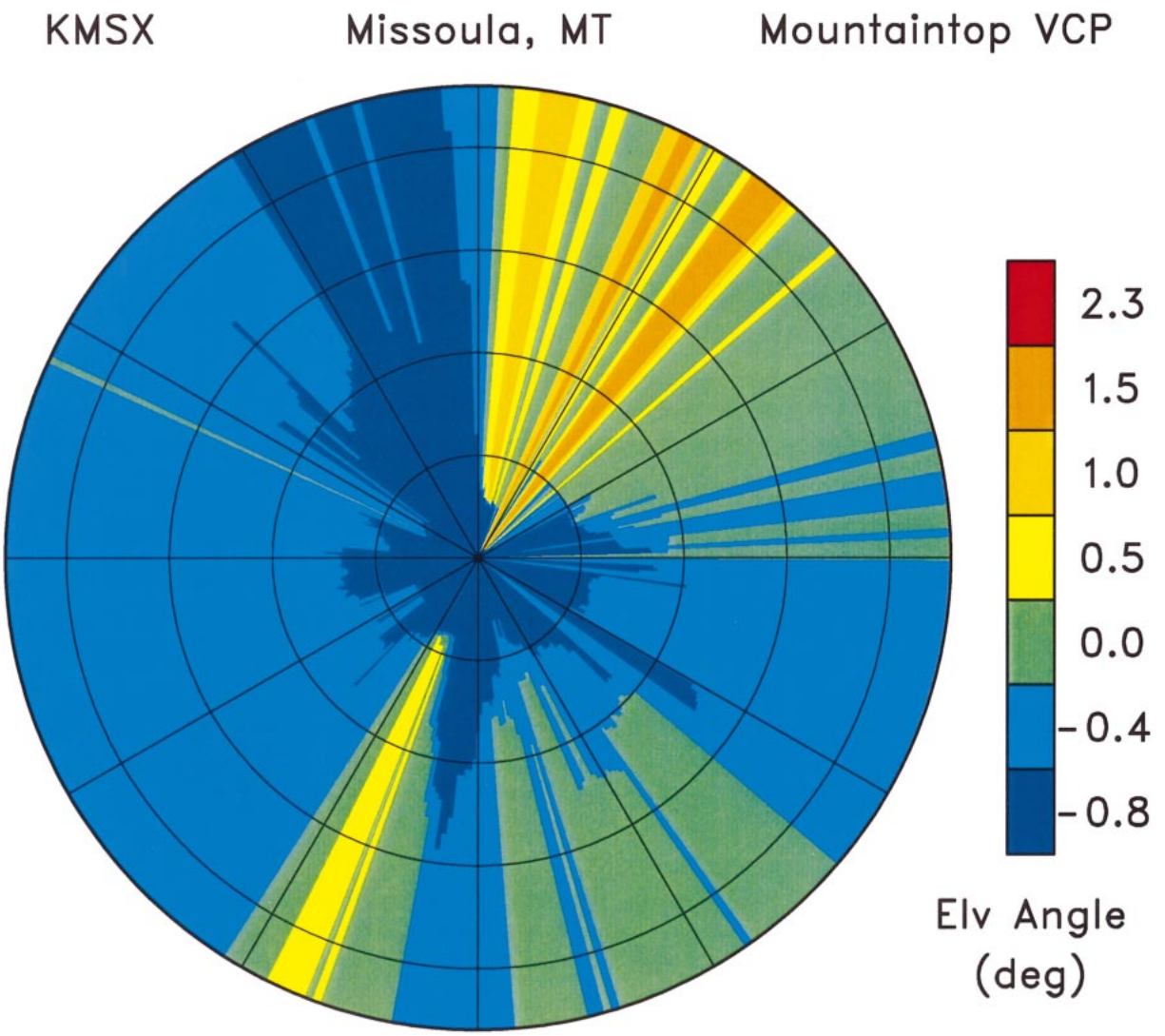

FIG. 4. Plot of lowest unblocked elevation angles (color coded on the right) within 230 km of simulated KMSX. Range circles are at 50-km intervals.

established limits for maximum permissible exposure. Radiation is considered to be safe for humans if the exposure level (power density) is less than 1 mW cm^{-2} averaged over any 30-min period (FCC 1996). As a safety factor, this guideline is nearly two orders of magnitude less than the 50–100 mW cm^{-2} exposure level at WSR-88D frequencies that has been found not to be harmful based on both animal studies and human experience (e.g., Sirmans and Bontempi 1994a). Expressions for computing WSR-88D power density as a function of range are derived in appendix C.

The radiation exposure level as a function of distance from a WSR-88D is plotted in Fig. 5. It is clearly evident from the figure that the average power density near the radar is over two orders of magnitude less than the FCC limit for maximum permissible exposure. The average power density drops off to 0.001 of the guideline at a distance of about 0.4 km, 0.0001 at 1.9 km, 0.000 01 at 5.5 km, and so on. Therefore, *a WSR-88D poses no radiation hazard for the general public.* The average power density (over a 30-min period) within a few tens of meters of the radar is about two orders of magnitude less than that received by someone using a cellular telephone for 0.5 h, with the antenna positioned 10 cm from his or her head (see, for example, Sirmans and Bontempi 1994b). The average power density 0.5 km from the radar is comparable to that received by a person standing 1.0 m in front of an operating microwave oven with the door closed (e.g., Sirmans and Bontempi 1994b).

4. Forecasting challenges

There are several forecasting challenges that face the Missoula National Weather Service Forecast Office aris-

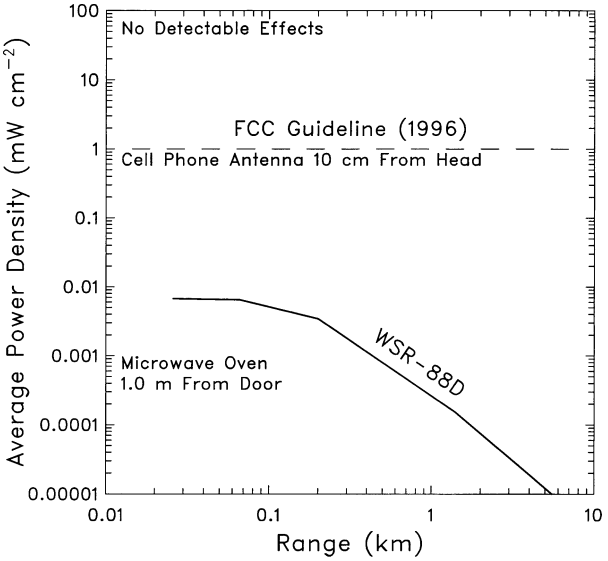

FIG. 5. WSR-88D radiation exposure levels (power density) as a function of range from the radar. The FCC (1996) safety guideline of 1.0 mW cm^{-2} averaged over a 30-min period is indicated by the dashed line. The portion of the WSR-88D curve within 1.37 km is based on field measurements and that beyond 1.37 km is based on Eq. (C5).

ing from the lack of negative elevation angles on the KMSX radar. One significant challenge deals with the onset of arctic blizzards. There is no way, at the present time, to determine when the leading edge of an arctic blizzard spills over the continental divide from the east and enters the Flathead River valley. Figures 2a and 3a show that under normal propagation conditions the lowest elevation angle for VCP 11 (and all other current VCPs) is several kilometers above the terrain. However, if negative elevation angles were used (Figs. 2b and 3b), the center of the lowest elevation angle would be within 0.5–1.0 km of the ground from 30 to over 150 km to the north of the radar and from 35 to over 100 km to the south. The use of negative elevation angles would permit the forecasters to detect and monitor blizzard conditions as they move southward through the Flathead and Bitterroot River valleys.

Another significant forecasting challenge concerns convective storms that form in the Flathead Lake recreational area about 70–110 km north to north-northwest of the radar in the Flathead River valley. The large lake acts as a heat source, especially in the autumn months, when cold air masses move over the warm lake. In these situations, significant convective storms can form that are too shallow to be detected using the current elevation angles, meaning that the storms are less than 2.5–3 km deep. These storms can be quite intense, occasionally developing waterspouts and strong wind gusts that can sink boats and cause damage to docks and lakeshore property. As shown in Fig. 2b, negative elevation angles would detect the boundary layer winds in the lowest 0.5–1.0 km and would help to detect and monitor the storms.

5. Improved weather detection

Following are simulations that show the types of detection improvements that could be expected using negative elevation angles. In each of these cases, the valley floor is represented by a horizontal plane 1.5 km below the radar.

a. Surface divergence/convergence

A short-term forecasting and warning challenge centers around the current inability of KMSX to detect either the presence of convergence along advancing fronts and surface outflow boundaries or the divergence associated with microburstlike phenomena. Figure 6a shows representative vertical profiles of idealized normalized divergence associated with convergence lines and microbursts. Since the profiles are mirror images of each other, their detection can be combined in Fig. 6b. Figure 6b shows the percentage of surface divergence that can be detected under normal propagation conditions in the surrounding valleys at the lowest elevation angle of each VCP. Since all of the activity is below the lowest elevation angle of VCP 11, nothing is detected. For the mountaintop VCP, as the lowest elevation angle approaches the simulated valley floor, up to 55% of surface divergence is detected. About 50% of the surface divergence is detected in the vicinity of Flathead Lake. More than one-third of the surface divergence is detectable between 55 and 170 km from the radar.

b. Vertically integrated liquid

For storms that have the potential of producing damage (hail, winds, tornadoes), vertically integrated liquid (VIL) is a radar-derived parameter that forecasters find useful (e.g., Kitzmiller et al. 1995; Amburn and Wolf 1997). VIL is a measure of the liquid water in a vertical column and is computed as a function of the vertical profile of reflectivity (Greene and Clark 1972). Owing to its vertically integrated properties, VIL provides a means for comparing the vertical resolution of various VCPs. The reflectivity profile in Fig. 7a is representative of maximum reflectivity within a modest-sized severe storm where graupel and hail are growing at midaltitudes prior to descent (e.g., Torgerson and Brown 1996). Since the profile is of the maximum reflectivity within a cell, the computed quantity is called cell-based VIL, in contrast to the more commonly used grid-based VIL. Cell-based VIL calculated for a storm with the reflectivity profile in Fig. 7a and a finescale vertical sampling interval of 0.1 km produces a cell-based VIL value of 34 kg m^{-2} (dashed line in Fig. 7b).

VIL computed using the mountaintop VCP under normal propagation conditions is essentially identical to the

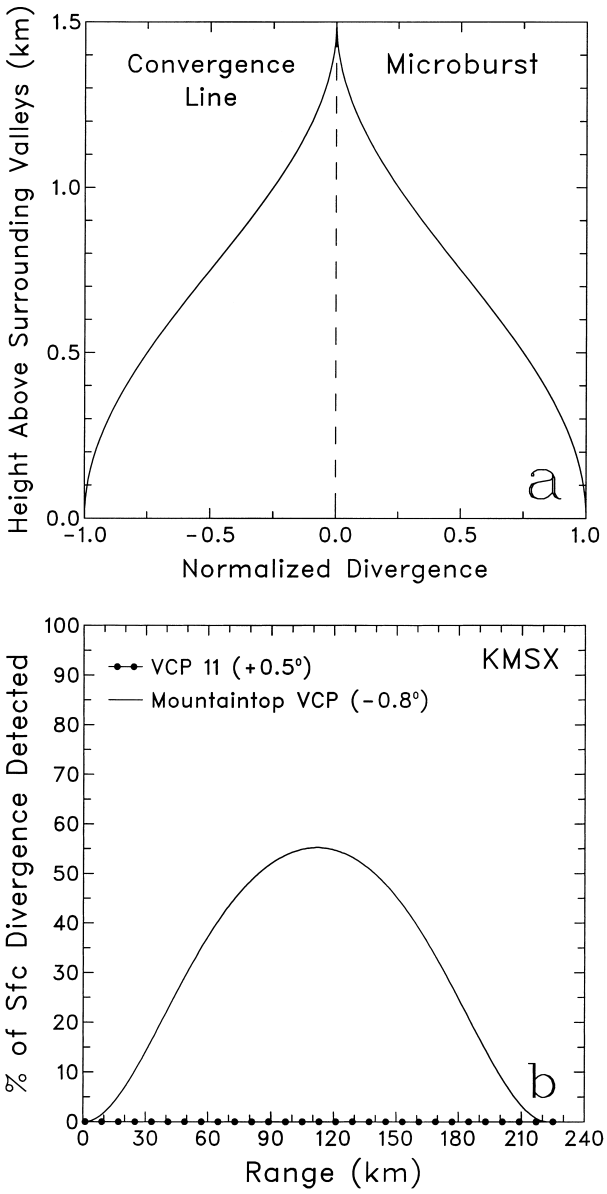

FIG. 6. Simulated low-altitude divergence. (a) Simulated divergence (normalized) profiles as a function of height for a convergence line and a microburst. (b) Percentage of the surface divergence detected at the lowest elevation angle for VCP 11 (dotted curve along abscissa) and the mountaintop VCP (solid curve). The radar is assumed to be 1.5 km above a plane surface that represents the valleys surrounding KMSX.

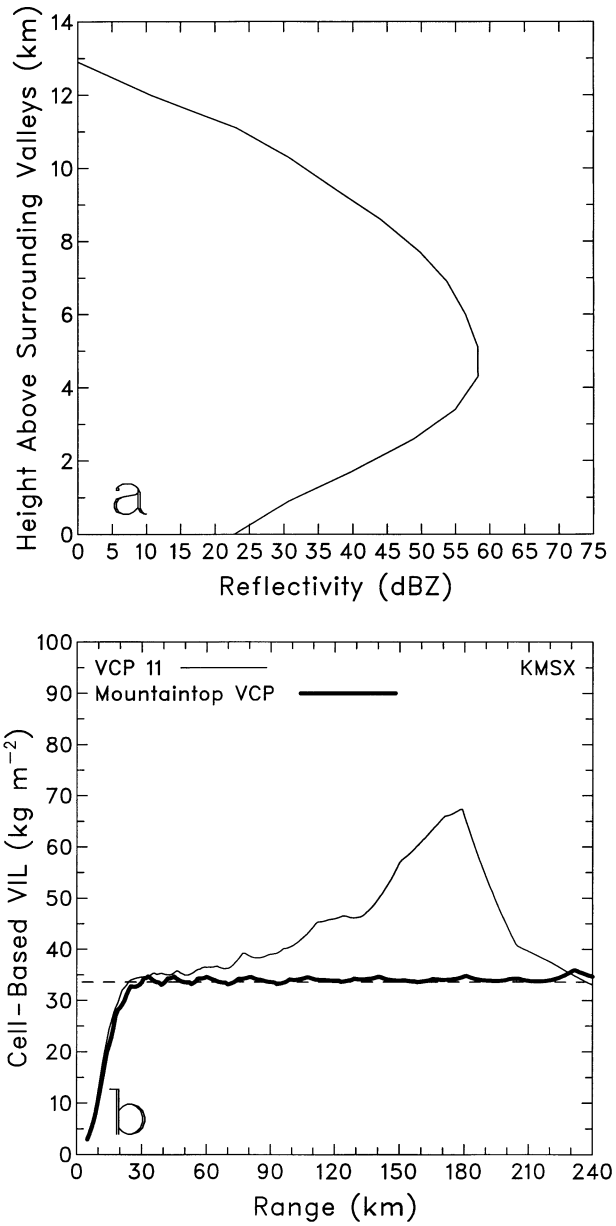

FIG. 7. Simulated cell-based VIL. (a) Vertical reflectivity profile in a simulated thunderstorm. (b) Comparison of simulated cell-based VIL for VCP 11 (thin curve) and the mountaintop VCP (thick curve). The true VIL value is indicated by the dashed line. The radar is assumed to be 1.5 km above a plane surface that represents the valleys surrounding KMSX.

true value from 25 to 240 km or more from the radar (Fig. 7b). Within 25 km of the radar, the elevation angles encompass only the lower portions of the storm (depth increases with range), so VIL is underestimated.

For VCP 11, the VIL values shown in Fig. 7b indicate that reliable values are computed only in the range interval from about 25 to 70 km. The overestimation of VIL beyond 70 km is a consequence of the vertical integration process. At each elevation angle, the maximum reflectivity within the storm is assigned to a depth (Δz) extending from halfway to the adjacent lower elevation angle to halfway to the adjacent higher elevation angle. The Δz interval for the reflectivity value at the lowest elevation angle extends down to the ground. So, as Δz increases with range, the height interval containing the largest reflectivity values carries an increasing amount of weight in computing VIL and thus the VIL value increases (e.g., Mahoney and Schaar 1993). With increasing range, VIL within the simulated storm con-

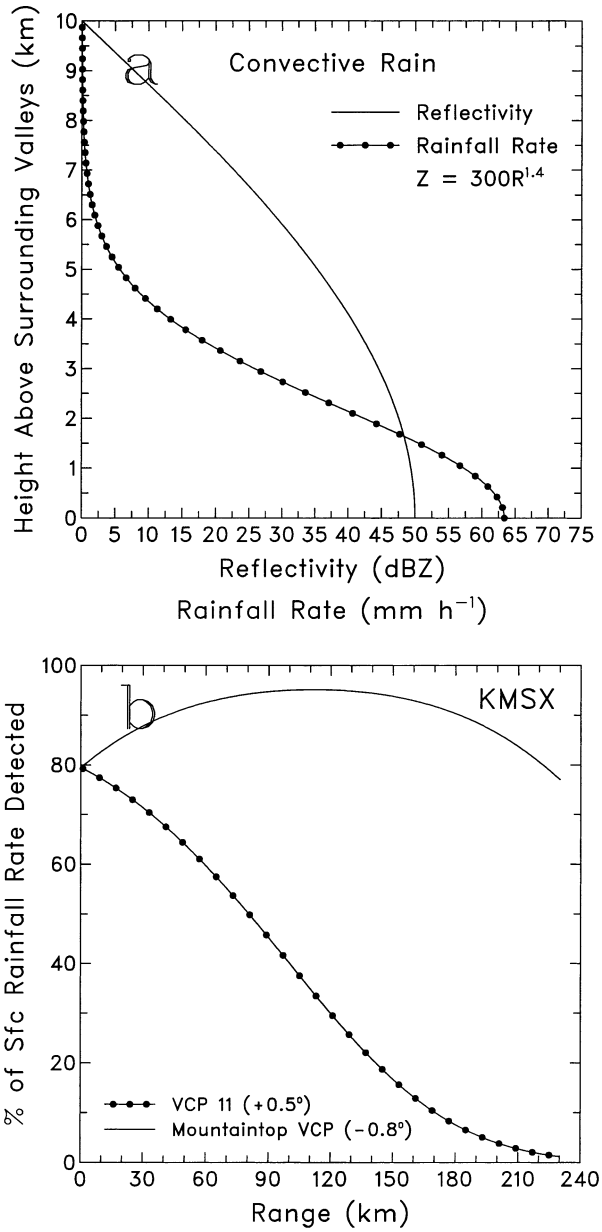

FIG. 8. Simulated convective rainfall rate. (a) Vertical profile of simulated rainfall rate (R) and the associated reflectivity (Z) profile. The reflectivity profile is based on vertical profiles of maximum reflectivity observed in convective storms at the time that maximum reflectivity is reaching the surface (e.g., Torgerson and Brown 1996). The rainfall rate value at a given height was computed from the reflectivity value at the same height using the indicated Z–R relationship. (b) Percentage of simulated surface rainfall rate detected at the lowest elevation angle for VCP 11 (dotted curve) and the mountaintop VCP (solid curve). The radar is assumed to be 1.5 km above a plane surface that represents the valleys surrounding KMSX.

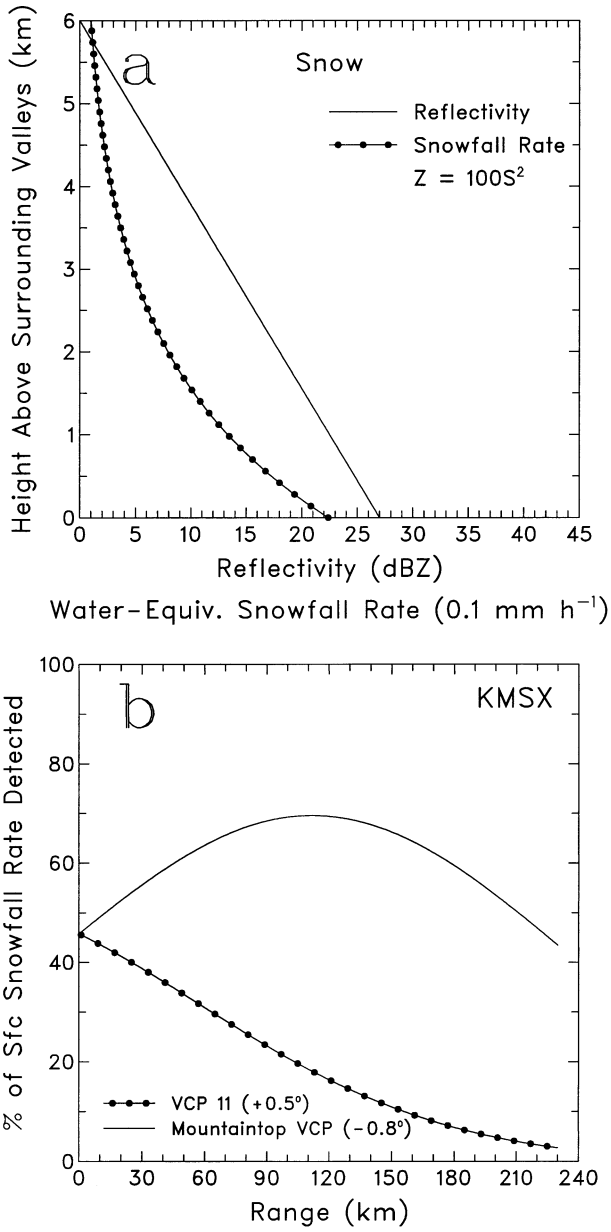

FIG. 9. Simulated snowfall rate. (a) Vertical profile of simulated water-equivalent snowfall rate (S) and the associated reflectivity (Z) profile. The snowfall rate value at a given height was computed from the reflectivity value at the same height using the indicated Z–S relationship. (b) Percentage of simulated surface water-equivalent snowfall rate detected at the lowest elevation angle for VCP 11 (dotted curve) and the mountaintop VCP (solid curve). The radar is assumed to be 1.5 km above a plane surface that represents the valleys surrounding KMSX.

tinues to increase until the height of the lowest elevation angle coincides with the layer of maximum reflectivity (at a range of 180 km in this example). As the storm moves beyond this range, there are a decreasing number of elevation angles sampling the storm and all of the elevation angles are above the maximum reflectivity layer, resulting in decreasing VIL values. An advantage of the mountaintop VCP is that the negative and more closely spaced lower elevation angles remain below the height of maximum reflectivity for a much greater distance and thus provide better vertical resolution than do the elevation angles with VCP 11.

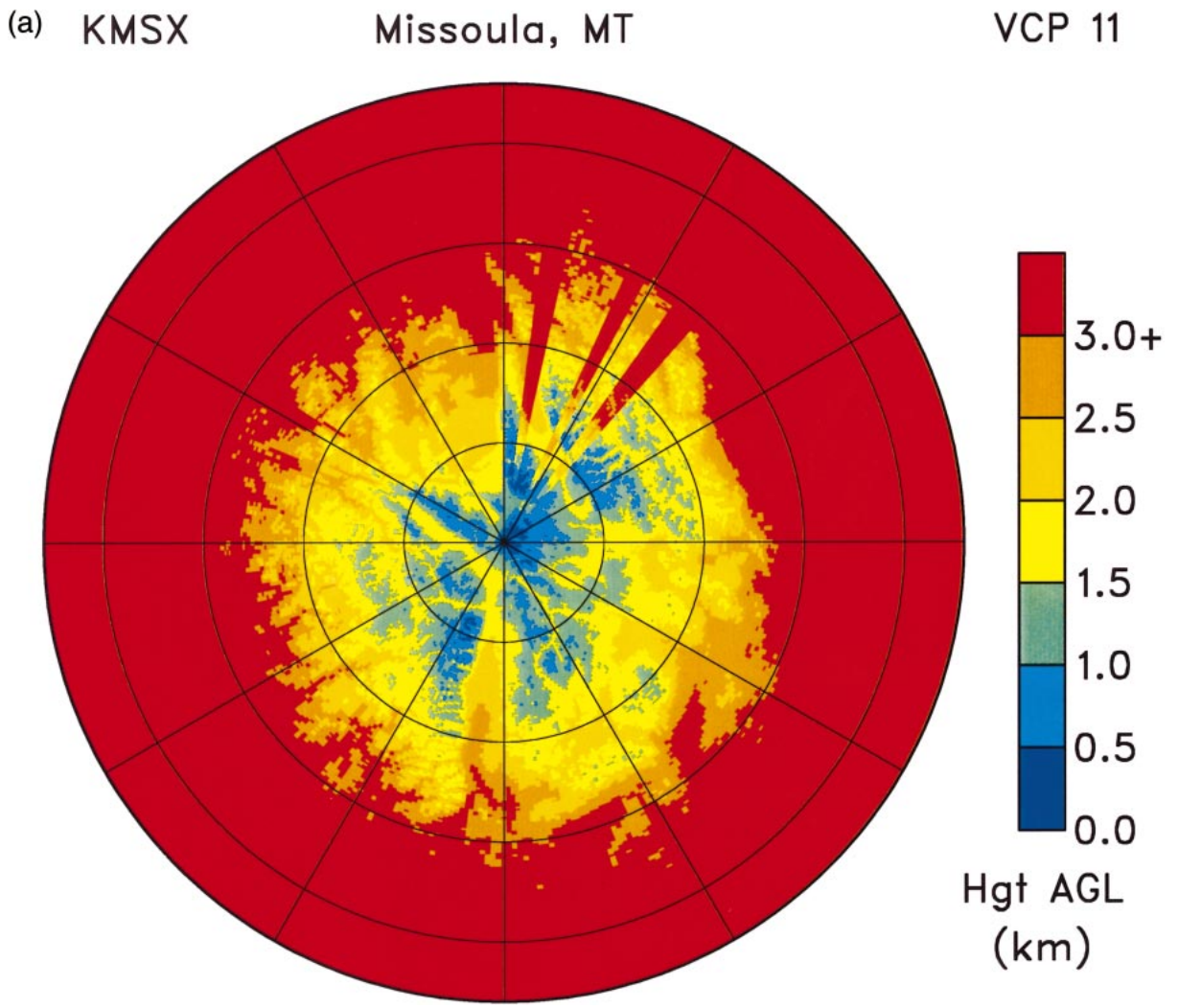

FIG. 10. Heights of the lowest unblocked beam above the underlying terrain within 230 km of KMSX for (a) VCP 11 and (b) mountaintop VCP. Range circles are at 50-km intervals.

c. Convective rain

A simulation of convective rainfall rate is shown in Figs. 8a and 8b. The assumed vertical profile of reflectivity in a convective storm (where rain is reaching the surface) and the profile of the associated rainfall rate based on the indicated relationship are found in Fig. 8a. Figure 8b shows the percentage of simulated surface rainfall rate that would be detected under normal propagation conditions in the surrounding valleys at the lowest elevation angle for the two VCPs. For VCP 11, 79% of the surface rate is measured near the radar, with the percentage of the surface rate decreasing to 50% at 80 km and to 20% at 140 km. On the other hand, the measured rainfall rate using the mountaintop VCP potentially is 77%–95% of the surface rate at all ranges within 230 km of the radar—a very impressive advantage due to the use of negative elevation angles.

d. Snowfall

Figure 9a shows a typical vertical profile of reflectivity (Z) in snow (e.g., Kingsmill and Huggins 1999) and the associated water-equivalent snowfall rate (S) based on the indicated Z–S relationship. Relative to a plane representing the valleys 1.5 km below the radar, Fig. 9b shows the percentage of the simulated surface snowfall rate that is measured at the lowest elevation angle for VCP 11 and for the mountaintop VCP under normal propagation conditions. Using VCP 11, the estimated snowfall rate rapidly decreases from 46% at the radar to about 20% at 100 km, to about 10% at 150 km, and approaches zero at farther ranges as the lowest elevation angle overshoots the precipitating clouds. However, the mountaintop VCP potentially measures 43%–70% of the surface snowfall rate over all of the surrounding valleys within 230 km of the radar. While the

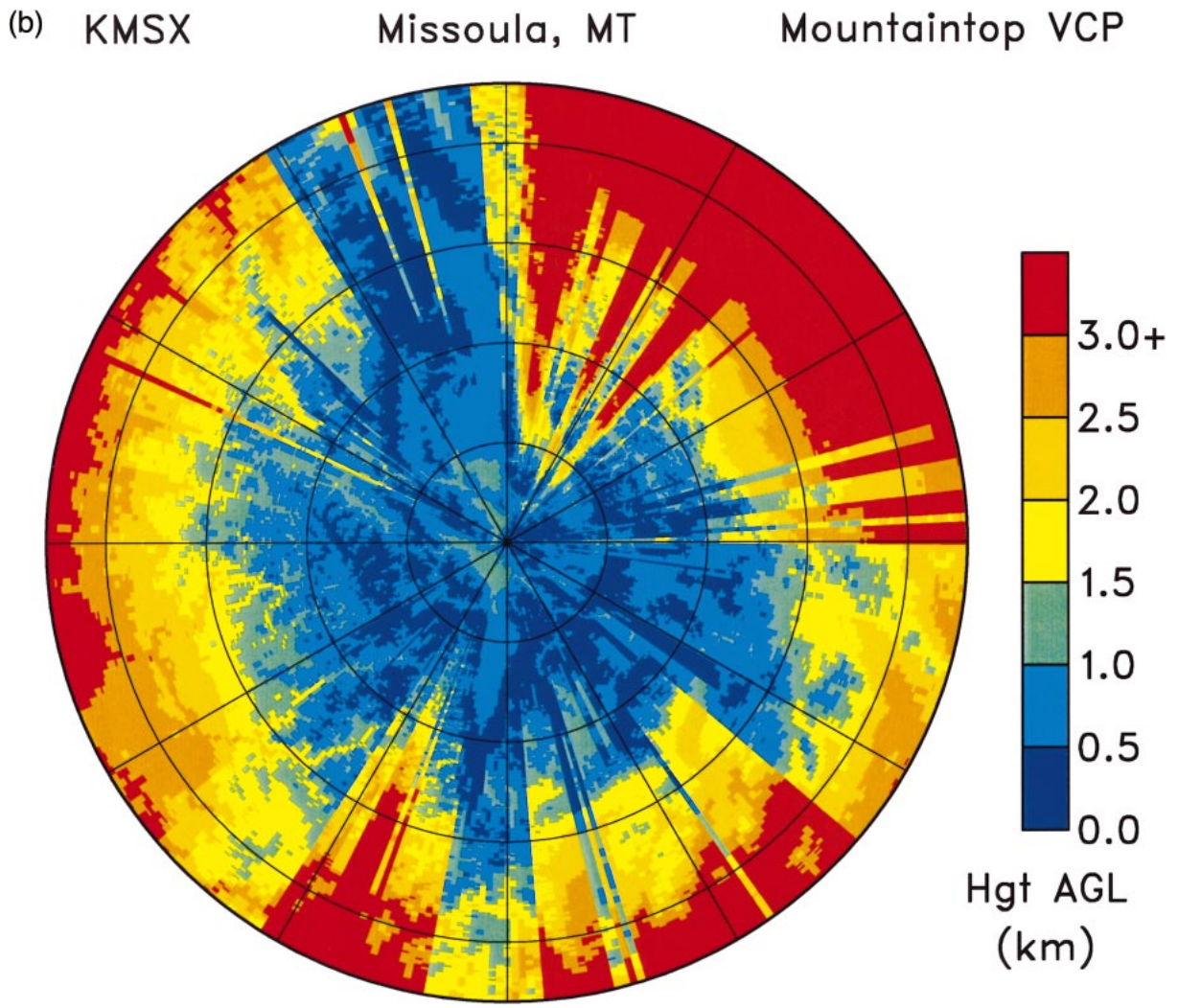

FIG. 10. (*Continued*)

use of negative elevation angles shows an improvement over VCP 11, the snowfall rate at the lowest negative elevation angle still is not a good approximation of snowfall at the surface. The types of techniques discussed in the next section will have to be applied in order to arrive at more credible surface snowfall estimates.

6. Precipitation over variable terrain

For the more general situation where the terrain is not flat, one would like to know how close the radar beam is to the terrain, especially for the estimation of surface precipitation. With the WSR-88D's current Precipitation Processing System (PPS), reflectivity at the (unblocked) elevation angle closest to 1 km above the terrain is used to compute a rainfall rate that is assumed to be constant from there down to the ground (e.g., Fulton et al. 1998). If the beam is an appreciable distance above the ground, the radar may provide a poor estimate. There is a provision in the PPS to use rain gauge data to adjust the radar estimates, but that provision has not yet been activated (e.g., Fulton et al. 1998). Another approach for getting a better estimate of surface precipitation would be to use an assumed vertical profile of reflectivity to extrapolate the reflectivity at the selected elevation angle to the ground (e.g., Joss and Waldvogel 1990; Andrieu and Creutin 1995; Seo et al. 2000).

All of these approaches would benefit from radar data being available close to the ground. Shown in Figs. 10a and 10b are the heights of the lowest unblocked beams above the terrain for the two VCPs. The terrain-relative heights for the conventional VCP 11 are shown in Fig. 10a. Only very limited portions of the terrain are within 1 km of an unblocked elevation angle, as indicated by the two shades of blue. Virtually all of the terrain beyond 130 km lies more than 3 km below the lowest unblocked

beam (nearly 70% of the area within 230 km of the radar). On the other hand, using the mountaintop VCP (Fig. 10b), nearly all of the terrain within 100 km, and some of it out to 230 km, is within 1 km of an unblocked elevation angle. The lowest unblocked beam is more than 3 km above the terrain for only about 25% of the 230-km coverage range. Therefore, the lower elevation angles of the mountaintop VCP would make it possible to compute more accurate rainfall estimates over a significant portion of the KMSX coverage area.

7. Summary and conclusions

The VCPs currently authorized for use with all WSR-88Ds specify that the lowest elevation angle is +0.5°. This specification, which was developed for flatland radars, is unsuited for mountaintop radars because the center of the lowest radar beam is several kilometers above the areas of concern to the local forecast office. With the lack of low-altitude data, rainfall and snowfall accumulations may not be accurately estimated and phenomena that produce low-altitude damaging winds may not be detected.

Looking down from an elevated position, a mountaintop radar provides a different perspective than is possible using a flatland radar. For the case of the flatland radar, the height of the radar beam increases with increasing range from the radar. However, for a mountaintop radar using negative elevation angles, the height of the radar beam decreases with range before starting to increase and thus provides an extensive range interval where the unblocked beam is close to the terrain.

Using basic radar considerations and the terrain features in the valleys surrounding KMSX, a sample volume coverage pattern was developed specifically for that radar. The VCP's lowest elevation angle of −0.8° permits the center of the radar beam to be within 0.5–1.0 km of the terrain up to distances of 100–150 km and more in the Flathead and Bitterroot River valleys. Simulations of representative meteorological conditions reveal a significant improvement (relative to the current VCPs) in radar detection of parameters of vital concern to forecasters.

The potential of microwave radiation hazards near the radar was investigated. Under routine operating conditions, the maximum exposure near the radar is two orders of magnitude less than the Federal Communications Commission's maximum permissible exposure level of 1 mW cm^{-2} averaged over 30 min, as well as being two orders of magnitude less than the exposure received by an individual using a cellular telephone. Therefore, a WSR-88D poses no radiation hazard for the general public.

Based on what was learned in this study, it is apparent that there would be significant benefits from the use of negative elevation angles at mountaintop radar sites in Alaska, Hawaii, and the western and northeastern portions of the contiguous United States. With negative elevation angles employed at mountaintop sites, forecasters would be able to alert the public of heavy snowfall and rainfall situations that otherwise could have gone undetected using the current volume coverage patterns. Most severe surface wind situations are relatively shallow and, without being able to use lower elevation angles to detect the existence of such phenomena, forecasters would be at a complete loss. Therefore, having radars that can scan at negative elevation angles in the mountainous regions of the United States would help the National Weather Service to accomplish its stated mission of protecting life and property in those parts of the country.

Acknowledgments. Dale Sirmans (RS Information Systems) was an invaluable source of information about the intricacies and operational capabilities of the WSR-88D. The authors appreciate comments on the manuscript by Drs. Kim Elmore and Jian Zhang (National Severe Storms Laboratory), among others. Comments by the anonymous reviewers helped to improve the manuscript. This study was funded by the National Severe Storms Laboratory.

APPENDIX A

Procedure for Developing a Mountaintop Volume Coverage Pattern for KMSX

The procedure for producing a tailored set of elevation angles for a mountaintop radar is discussed below. The procedure involves determining (a) a minimum elevation angle that adequately covers valley population centers and (b) a set of additional elevation angles that provide adequate vertical resolution during a reasonable time interval. The population centers in the valleys surrounding KMSX are about 1.5 km below the radar.

a. Determining lowest elevation angle

Determination of the lowest elevation angle is based on a theoretical study by Smith (1998). He found that when the center of the radar beam is about 0.3 beamwidth above the flat ground, there is an acceptable balance between loss of power received from low-altitude features and the increase in ground clutter. KMSX has an antenna pattern half-power beamwidth of about 0.87°, so 0.3 beamwidth is 0.26°. For this study, a rounded value of 0.3° was used as the vertical angular distance between the ground and the center of the lowest elevation angle.

As indicated in Fig. A1, the initial step in determining the lowest elevation angle was to compute the negative elevation angle (called the grazing angle) that is tangent to a horizontal plane 1.5 km below the radar. Through an iterative process, it was determined that −1.1° was the elevation angle where the center of the beam was tangent to the plane. Adding 0.3° to the grazing angle

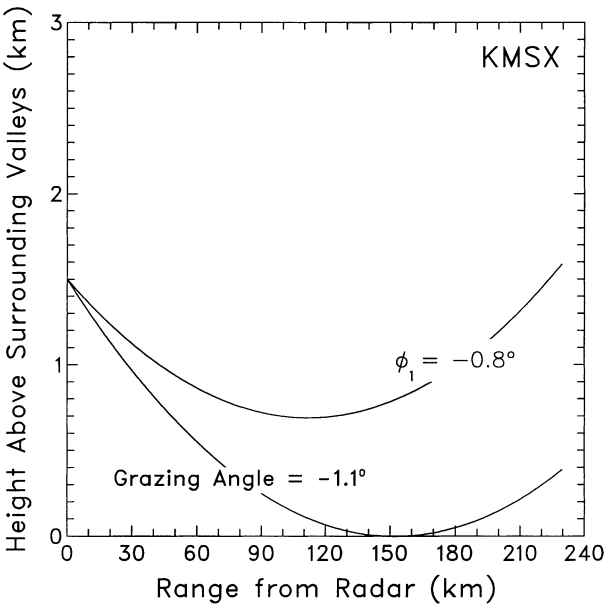

FIG. A1. Procedure for computing the lowest elevation angle. The grazing angle is the elevation angle that is tangent to a plane 1.5 km below the radar (representing the valleys surrounding KMSX). The lowest elevation angle (ϕ_1) is defined as being 0.3° above the grazing angle.

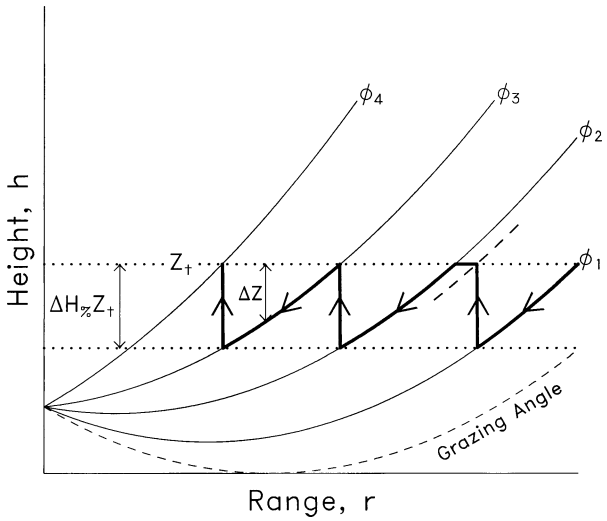

FIG. A2. Schematic of the process used to compute elevation angles for a simulated mountaintop VCP. See text for details.

produced an angle of −0.8° as the center of the beam for the lowest elevation angle (ϕ_1).

The paths of the radar beams in Fig. A1 were computed using Eq. (9.8) of Doviak and Zrnić (1993). These computations are based on standard conditions for the index of refraction (e.g., Battan 1973). Nonstandard conditions that exist when low-altitude situations, such as nocturnal radiational cooling and post–cold frontal passage, occur in the valleys are not considered for these computations. [In nonstandard situations, the resulting inversion leads to anomalous propagation (AP), where any radar beam that enters the inversion layer bends downward and intercepts the ground.]

b. Determining the other elevation angles

The rest of the elevation angles in the volume coverage pattern were determined using a mountaintop radar version of the optimization technique discussed by Brown et al. (2000) and illustrated in Fig. A2. Having selected the lowest elevation angle ϕ_1, a height Z_t is specified and the corresponding distance from the radar is computed. The procedure is to decrease the range at that elevation angle until the height has decreased by an amount equal to a specified height interval percentage $\Delta H_\%$ (usually 15%–30%) of the initial height. At that range, the next elevation angle ϕ_2 is computed at the original height Z_t. If the difference between the two adjacent elevation angles is less than a specified amount (usually one-half to one vertical beamwidth), the range is decreased at constant height until the desired elevation angle difference is achieved. Then the process of decreasing range at constant elevation angle is repeated until the percentage height difference is met, and so on. In this way, a set of elevation angles is determined where most of the angles are separated by the same vertical distance at a given height above the ground. Since the vertical distance is a percentage of height, the distance between elevation angles decreases with decreasing height. This approach produces a set of elevation angles that are closest together at low elevation angles (providing good resolution at far ranges) and become progressively farther apart with height.

There is a trade-off between vertical resolution and temporal resolution. The more elevation angles there are, the better the vertical resolution, but the longer it takes to complete a volume scan. To resolve rapidly evolving phenomena, one would like to have the volume scans as short in time as possible. For optimum rotation rates, this trade-off is controlled through the specification of $\Delta H_\%$ and the maximum elevation angle.

Within a given volume scan, WSR-88D radars traditionally employ three different modes of operation in order to handle various data problems (see Table A1). For each elevation angle less than about 2.0°, the antenna makes two separate scans (each with a different pulse repetition frequency, PRF) in order to properly handle ground clutter suppression and to unfold range-folded echoes. During the first scan, reflectivity data (contiguous reflectivity mode using a low PRF) are processed and during the second scan, Doppler velocity data (contiguous Doppler mode using a higher PRF) are processed. Between elevation angles of 2.0° and 7.0°, reflectivity and Doppler velocity are collected in an interlaced ''batch'' mode (alternating between low and high PRFs) that permits the unfolding of range-folded echoes. For elevation angles above 7.0°, where range folding is unlikely, reflectivity and Doppler velocity

TABLE A1. Criteria used to estimate the time for completing a volume scan using a mountaintop VCP. About 0.4 min are added to the rotation rate time to account for algorithm computations following the completion of the volume scan.

Elevation angle above radar (°)	Rotation rate (rpm)	Standard error of estimate	Mode
≤2.0	3.5	0.55 dB	Contiguous reflectivity
	4.0	0.95 m s^{-1}	Contiguous Doppler
2.0–7.0	4.5	0.64 dB, 1.1 m s^{-1}	Batch
>7.0	4.8	0.65 dB, 1.0 m s^{-1}	Contiguous Doppler

data are collected using the higher PRF contiguous Doppler mode.

For the case of the KMSX simulation, the above elevation angle criteria also were used because the negative elevation angles, and some of the positive ones, will encounter some of the surrounding terrain, as well as range folding. The VCP developed here assumes that the radar computes reflectivity, mean Doppler velocity, and spectrum width values every 1.0° in the azimuthal direction as the antenna rotates. It also takes advantage of the fact that WSR-88Ds can rotate up to five revolutions per minute (rpm) without significantly compromising the requirements for standard errors of estimate for reflectivity to be less than about 1 dB and for Doppler velocity to be less than about 1 m s^{-1}. The rotation rates and associated standard errors of estimate listed in Table A1 are not those used by operational WSR-88Ds, but are values used in this study to improve the trade-off between vertical resolution and temporal resolution.

Before determining the other elevation angles of a sample VCP for KMSX, a value for the percentage height difference ($\Delta H_{\%}$) between adjacent elevation angles had to be specified. An example of trade-offs between temporal resolution and vertical resolution in the selection of the percentage height difference for flatland radars is given in Table 1 of Brown et al. (2000). For the current example, a value of 26% was chosen for $\Delta H_{\%}$, Z_t was set at 10 km, and the minimum angle increment between adjacent elevation angles was chosen to be one-half beamwidth or 0.44°. The resulting VCP scans 14 distinct elevation angles between −0.8° and +21.3° in 5 min. Height–range plots of these elevation angles are shown in Figs. 2b and 3b.

APPENDIX B

Calculation of Radar Beam Blockage

The procedure for calculating the amount of radar beam blockage due to terrain features is discussed in this appendix. It is conventional for the width of a radar beam to be defined as the width where the power falls off to one-half of the peak power (called the one-way half-power beamwidth, BW). To compute the amount of blockage, however, one wants to consider the entire main lobe of the beam, which is about 3 times the half-power beamwidth. The distribution of power across the main lobe can be approximated by the following circularly symmetric Gaussian one-way antenna pattern (e.g., Sirmans 1993), which is plotted in Fig. B1:

$$W = \exp\left[-\frac{(r\mathrm{BW})^2}{2\sigma^2}\right], \tag{B1}$$

where r ranging from 0.0 to 1.5 is a fractional half-power beamwidth, BW, to indicate radial distance outward from the center of the main lobe and

$$\sigma^2 = \frac{(\mathrm{BW})^2}{8\ \ln 2} \tag{B2}$$

is the variance of the Gaussian pattern.

For the purpose of computing the percentage of the radar beam that is blocked by terrain, the cross section normal to the center axis of the main lobe was divided into 15 equally spaced annuli, as illustrated in Fig. B2. The diameter of the main lobe is assumed to be 3 BW, with each annulus having a radial width of 0.1 BW. The objective is to determine the percentage of beam blockage in the main lobe, as expressed by

$$\% = \frac{X}{Y} \times 100, \tag{B3}$$

where X is the power-weighted area intercepted by the

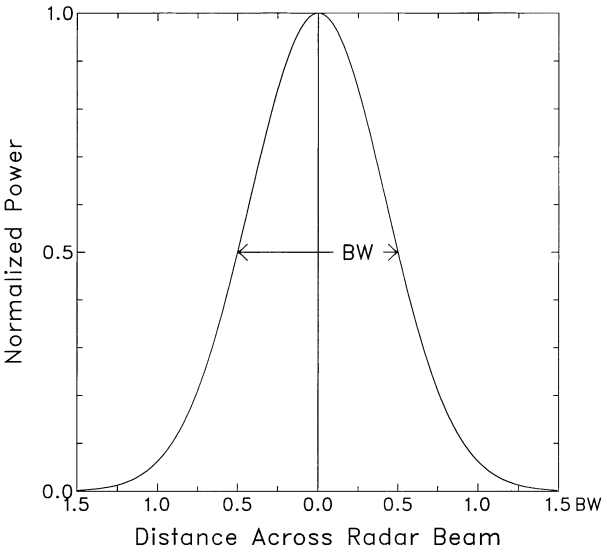

FIG. B1. Normalized power across the main lobe of a WSR-88D, approximated by the Gaussian distribution expressed in Eq. (B1). The half-power beamwidth is indicated by BW.

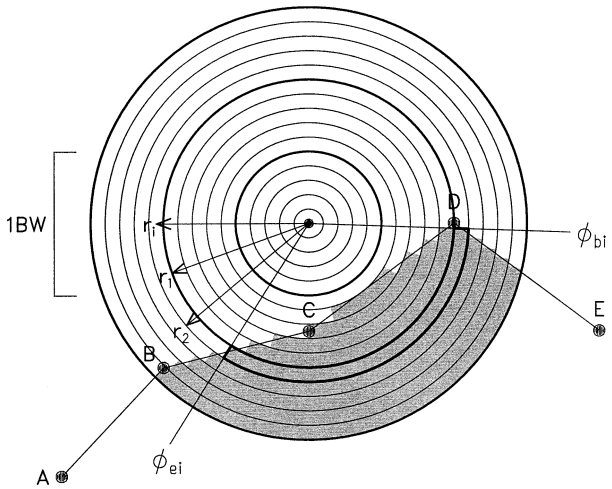

FIG. B2. Illustration of the procedure used to compute the percentage of beam blockage. The cross section normal to the axis of the main lobe is divided into 15 equally spaced annuli. The thicker circles represent diameters of 1, 2, and 3 half-power beamwidths (*BW*). The shaded area beneath the ABCDE curve represents terrain partially blocking the beam. The various parameters are defined in the text.

terrain and Y is the power-weighted area within the entire main lobe.

The quantity X in Eq. (B.3) is the sum of the power-weighted annulus segments that are blocked by the terrain (one such segment is indicated by the bold outline in Fig. B2), as given by

$$X \equiv \sum_{i=1}^{N} \frac{\pi}{360}(\phi_{ei} - \phi_{bi})[(r_2\mathrm{BW})^2 - (r_1\mathrm{BW})^2]_i W_i, \quad \text{(B4)}$$

where N is the number of annuli ($1 \le N \le 15$) intercepted by the terrain, ϕ_{bi} and ϕ_{ei} are the beginning and ending angles bounding the blocked segment of the ith annulus ($\phi_{bi} < \phi_{ei}$ with the angles being defined as positive in a clockwise direction from the top of the beam), and r_1 and r_2 are the radial limits of the ith annulus. The weighting function W_i is the normalized power at the middle of the ith annulus, given by

$$W_i = \exp\left[-\frac{(r_i\mathrm{BW})^2}{2\sigma^2}\right], \quad \text{(B5)}$$

where r_i is the radius at the middle of the ith annulus.

The quantity Y is the total power-weighted area within the main lobe, expressed as the sum of the power-weighted areas of all 15 annuli:

$$Y \equiv \sum_{i=1}^{15} \pi[(r_2\mathrm{BW})^2 - (r_1\mathrm{BW})^2]_i W_i. \quad \text{(B6)}$$

For precipitation processing, the WSR-88D precipitation algorithm assumes the beam is completely blocked when at least 60% of the beam is blocked (e.g., Fulton et al. 1998).

APPENDIX C

Determination of WSR-88D Radiation Hazards

Since a WSR-88D is a source of microwave radiation, it is important to determine whether it poses a radiation threat to the general public (e.g., Sirmans and Bontempi 1994a). Outside the radar enclosure, the only potential hazard arises from *nonionizing* radiation that causes a slight increase in body temperature. At power density levels greater than 100 mW cm^{-2}, a microwave oven cooks food by transferring energy to water molecules in the food (e.g., Cleveland and Ulcek 1999). The resulting heating rate of the tissue is too fast for the food to dissipate the heat, so the temperature increases. At lower power density levels, there is no cumulative effect from nonionizing radiation within the human body because blood circulation dissipates the slight temperature increase that can arise. [On the other hand, *ionizing* radiation, such as X rays, can produce molecular changes that can lead to damage to biological tissues, including DNA (Cleveland and Ulcek 1999).]

In order to prevent humans from being subjected to significant increases in body temperature, a series of radiation exposure guidelines have been specified over the years. The most recent and most conservative U.S. limit for maximum permissible exposure, established by the FCC (1996), is a power density level of 1 mW cm^{-2} averaged over any 30-min period. The Canadian Safety Code 6 specifies that the average power density over a 6-min period also should not exceed 1 mW cm^{-2} (Radiation Protection Bureau 1999). These guidelines are 1%–2% of a power density level that has been found not to be harmful based on both animal studies and human experience. Using an older radiation guideline of an average of no more than 2 mW cm^{-2} over a 6-min period, Sirmans and Bontempi (1994a) discuss a worst-case scenario of human exposure. At the guideline power density level of 2 mW cm^{-2}, the rise in body temperature for an average-sized man would be only 0.0037°C, *if* the body were not able to dissipate the heat. With the human body being able to dissipate heat, the rise in body temperature is much less than 0.0037°C. Radiation exposure guidelines perform a valuable service by limiting public exposure to levels having negligible heating effects.

In this appendix, the power density at the center of the radar beam as a function of range from a WSR-88D is compared with the FCC standard. The variation of power density with range behaves differently near the radar and farther away. The range that separates the ''near field'' from the ''far field'' is

$$R = \frac{2D^2}{\lambda} = 1.37 \text{ km}, \quad \text{(C1)}$$

where D is the diameter of the antenna (8.5 m) and λ is the average wavelength of WSR-88Ds (10.56 cm). Variation of the power density in the near field is based

on power measurements and variation in the far field is based on the equations developed below.

Following the development of Sirmans and Bontempi (1994a), the typical far-field peak power density, D_p, for continuous transmission along the center of the antenna pattern main lobe can be computed from the radar equation:

$$D_p = \frac{P_p G}{4\pi R^2} = \frac{1.621 \times 10^{12}\ \text{mW}}{R^2\ (\text{cm}^2)}, \qquad \text{(C2)}$$

where P_p is the peak power radiated by the antenna (500 kW; 750 kW is the peak output of the transmitter), G is the antenna gain (46.1 dB), and R is range (cm) from the radar. In actuality, power is not transmitted continuously, but in pulses. Consequently, the fraction of the time that the WSR-88D transmitter is transmitting a pulse is a maximum of only 0.002. The average power density, D_T, transmitted from the beginning of one pulse to the beginning of the next pulse for a stationary antenna then is

$$D_T = 0.002 D_p = \frac{3.242 \times 10^{9}\ \text{mW}}{R^2\ (\text{cm}^2)}. \qquad \text{(C3)}$$

The average power density given in Eq. (C3) is the amount that one would encounter if the radar antenna were stationary with the center of the beam pointing at a fixed point. This power density level is not experienced with the WSR-88D because, when the antenna stops rotating, there is an elaborate safety interlock system that switches the transmitter off after 5 min.

With a rotating antenna, the average power density encountered at a given point in space is significantly less than that hypothetically encountered with a stationary antenna. For one 360° rotation of an antenna having a typical half-power beamwidth of 0.89°, the corresponding equal-energy beamwidth is 0.67°, where the equal-energy beamwidth is a rectangular distribution having the same energy and peak power as the antenna's Gaussian distribution. The average power density received at a point is 0.67°/360° or 0.001 86 of what would have been received if the center of a stationary beam were directed toward that point. Thus the average power density received at a given point from an antenna rotating at a fixed elevation angle is

$$D_\theta = 0.001\ 86 D_T = \frac{6.03 \times 10^{6}\ \text{mW}}{R^2\ (\text{cm}^2)}. \qquad \text{(C4)}$$

Since a volume coverage pattern consists of a series of 360° scans at specified elevation angles, not all of the elevation scans will affect a point. Most of the power within a beam is within ±1° of the beam center. Therefore, the portion of a volume coverage pattern that would cause concern would be the lowest 2°. For the current VCPs and the example shown for KMSX, during any 30-min period the antenna does not spend more than 50% of the time pointing at elevation angles below 2° (a very conservative estimate). Therefore, the average power density received at a given point near the ground from an antenna rotating in a volume coverage pattern is

$$D_V = 0.5 D_\theta = \frac{3.015 \times 10^{6}\ \text{mW}}{R^2\ (\text{cm}^2)}. \qquad \text{(C5)}$$

Plotted in Fig. 5 is the power density curve for WSR-88Ds. The far-field portion of the curve (beyond 1.37 km) is based on Eq. (C5). The near-field portion of the curve is adjusted from actual near-field measurements made with a stationary antenna (e.g., Sirmans and Bontempi 1994a) using the same conversion factors ($0.001\ 86 \times 0.5 = 0.000\ 93$) that were used to derive Eq. (C5) from Eq. (C3).

It is clear from Fig. 5 that the general public has no basis for concern about harmful radiation coming from a WSR-88D. The curve indicates that the maximum exposure level is two orders of magnitude less than the FCC guideline, which itself is about two orders of magnitude less than a level that has been shown to produce no harmful effects (e.g., Sirmans and Bontempi 1994a). The microwave radiation received from a WSR-88D over a 0.5-h period is at least two orders of magnitude less than that received over the same time period from a cellular telephone antenna located 10 cm away from one's head.

REFERENCES

Amburn, S. A., and P. L. Wolf, 1997: VIL density as a hail indicator. *Wea. Forecasting,* **12,** 473–478.

Andrieu, H., and J. D. Creutin, 1995: Identification of vertical profile of radar reflectivity for hydrological applications using an inverse method. Part I: Formulation. *J. Appl. Meteor.,* **34,** 225–239.

Battan, L. J., 1973: *Radar Observation of the Atmosphere.* 3d ed. University of Chicago Press, 324 pp.

Brown, R. A., V. T. Wood, and D. Sirmans, 2000: Improved WSR-88D scanning strategies for convective storms. *Wea. Forecasting,* **15,** 208–220.

Cleveland, R. F., Jr., and J. L. Ulcek, 1999: Questions and answers about biological effects and potential hazards of radiofrequency electromagnetic fields. OET Bull. 56, 4th ed., Office of Engineering and Technology, 36 pp. [Available from Office of Engineering and Technology, Federal Communications Commission, Washington, DC 20554; also online at http://www.fcc.gov/rfsafety.]

Crum, T. D., R. L. Alberty, and D. W. Burgess, 1993: Recording, archiving, and using WSR-88D data. *Bull. Amer. Meteor. Soc.,* **74,** 645–653.

Doviak, R. J., and D. S. Zrnić, 1993: *Doppler Radar and Weather Observations.* 2d ed. Academic Press, 562 pp.

FCC, 1996: Guidelines for evaluating the environmental effects of radiofrequency radiation. *Federal Register,* 7 August, Vol. 61 (153), 41 006–41 019.

Fulton, R. A., J. P. Breidenbach, D.-J. Seo, D. A. Miller, and T. O'Bannon, 1998: The WSR-88D rainfall algorithm. *Wea. Forecasting,* **13,** 377–395.

Greene, D. R., and R. A. Clark, 1972: Vertically integrated liquid: A new analysis tool. *Mon. Wea. Rev.,* **100,** 548–552.

Joss, J., and A. Waldvogel, 1990: Precipitation measurement and hydrology. *Radar in Meteorology,* D. Atlas, Ed., Amer. Meteor. Soc., 577–606.

Kingsmill, D. E., and A. W. Huggins, 1999: Quantitative precipitation

estimates from a mountain-top WSR-88D: The 1997 New Year's flood. Preprints, *29th Int. Conf. on Radar Meteorology,* Montreal, QC, Canada, Amer. Meteor. Soc., 713–716.

Kitzmiller, D. H., W. E. McGovern, and R. E. Saffle, 1995: The WSR-88D severe weather potential algorithm. *Wea. Forecasting,* **10,** 141–159.

Leone, D. A., R. M. Endlich, J. Petričeks, R. T. H. Collis, and J. R. Porter, 1989: Meteorological considerations used in planning the NEXRAD network. *Bull. Amer. Meteor. Soc.,* **70,** 4–13.

Mahoney, E. A., and R. Schaar, 1993: WSR-88D scan strategy impacts on the vertically integrated liquid product. Preprints, *26th Int. Conf. on Radar Meteorology,* Norman, OK, Amer. Meteor. Soc., 44–46.

Radiation Protection Bureau, 1999: Safety code 6—Limits of human exposure to radiofrequency electromagnetic fields in the frequency range from 3 kHz to 300 GHz. Rep. 99-EHD-237, Environmental Health Directorate, Radiation Protection Bureau, Health Canada, 75 pp. [Available online at http://www.hc-sc.gc.ca/rpb.]

Seo, D.-J., J. Breidenbach, R. Fulton, D. Miller, and T. O'Bannon, 2000: Real-time adjustment of range-dependent biases in WSR-88D rainfall estimates due to nonuniform vertical profile of reflectivity. *J. Hydrometeor.,* **1,** 222–240.

Sirmans, D., 1993: Site-unique volume control patterns in the WSR-88D. Report to the NEXRAD Operational Support Facility, Titan Corp., 76 pp. [Available from WSR-88D Radar Operations Center, 1200 Westheimer Drive, Norman, OK 73069.]

—— and P. Bontempi, 1994a: WSR-88D radiation and biological system considerations. Report to the NEXRAD Operational Support Facility, Titan Corp., 121 pp. [Available from WSR-88D Radar Operations Center, 1200 Westheimer Drive, Norman, OK 73069.]

—— and ——, 1994b: Public information on NEXRAD WSR-88D radar microwave radiation. Report to the NEXRAD Operational Support Facility, Titan Corp., 17 pp. [Available from WSR-88D Radar Operations Center, 1200 Westheimer Drive, Norman, OK 73069.]

Smith, P. L., 1998: On the minimum useful elevation angle for weather surveillance radar scans. *J. Atmos. Oceanic Technol.,* **15,** 841–843.

Torgerson, K. L., and R. A. Brown, 1996: Radar signatures of updrafts within the Carson, ND hailstorm of 11 July 1989. Preprints, *18th Conf. on Severe Local Storms,* San Francisco, CA, Amer. Meteor. Soc., 81–85.